LAWRENCE
LIVERMORE
NATIONAL
LABORATORY

UCRL-CONF-229010

Lethality Effects of a High-Power Solid-State Laser

C. Boley, S. Fochs, A. Rubenchik

March 13, 2007

Directed Energy Symposium
Monterey, CA, United States
March 18, 2007 through March 23, 2007

Lethality Effects of a High-Power Solid-State Laser*

C. D. Boley[1], S. N. Fochs[2], and A. M. Rubenchik[3]
University of California
Lawrence Livermore National Laboratory
Livermore, CA 94551

We study the material interactions of a 25-kW solid-state laser, in experiments characterized by relatively large spot sizes (~3 cm) and the presence of airflow. The targets are 1-cm slabs of iron or aluminum. In the experiments with iron, we show that combustion plays an important role in heating the material. In the experiments with aluminum, there is a narrow range of intensities within which the material interactions vary from no melting at all to complete melt-through. A paint layer serves to increase the absorption. We explain these effects and incorporate them into a comprehensive computational model.

Keywords: solid-state laser, high average power, lethality, airflow, combustion.

Nomenclature

C	specific heat
I	laser intensity
T	temperature
T_c	combustion initiation temperature
U_0	wind speed
x_o	thickness of oxide layer
α	optical absorptivity
η	shear viscosity
κ	thermal conductivity
ρ	density
σ	shear stress

1. Introduction

Solid-state lasers with high average power are of great current interest. Our laboratory at LLNL has been developing such lasers for defense applications during the last ten years. Our most advanced device[9,10] contains four diode-pumped ceramic Nd:YAG slabs, producing

*Work performed under the auspices of the U.S. Department of Energy by the University of California, Lawrence Livermore National Laboratory, under Contract No. W-7405-ENG-48.
[1]E-mail address: boley1@llnl.gov; telephone: (925) 423-7365; fax: (925) 422-8297.
[2]E-mail address: fochs1@llnl.gov, telephone: (925) 422-2976.
[3]E-mail address: rubenchik1@llnl.gov; telephone: (925) 422-6131.

approximately 25 kW of average power at a wavelength of 1.053 μm. Routine operation for 10 seconds has been achieved. The laser operates at a pulse repetition rate of 200 Hz, producing pulses of energy about 125 J and length about 0.5 ms, for a duty factor of 10%. With the addition of another slab and an increased diode duty factor, the laser has also demonstrated 67 kW for 0.25 s.

During lasing operations, our lasers store waste heat in the solid-state slabs. In field applications, the hot slabs would be rapidly cooled or interchanged with cool slabs. Thus the devices are termed solid-state heat-capacity lasers (SSHCLs).

The material interactions of these lasers, including high-explosive initiation, have been explored at some length[1-6]. Since the thermal conduction length between pulses is small compared to typical target dimensions, the macroscopic heat distribution is readily seen to be governed by the time-average power[5]. Our predictive capability is embodied in a computational model (THALES[5]). Devices operating near 100 kW have been projected to be effective in defense against mortars[4,5] and Katyusha rockets[6].

Here we extend the material interaction studies to thick (1 cm) iron and aluminum coupons. The spot sizes are relatively large (~3 cm), and high-speed airflow is present. The irradiation time is 5 s. The experimental setup near the target is shown in Fig. 1. In the case of iron, we demonstrate that, under these conditions, combustion plays an important role in facilitating material heating. We have incorporated this in our modeling. For aluminum, we find a strong dependence on spot size, and therefore on incident intensity. At about 3 kW/cm^2, no melting is observed. At twice this intensity, however, the coupon rapidly melts through. We explain this behavior in terms of the large thermal conductivity. The behavior is altered by the

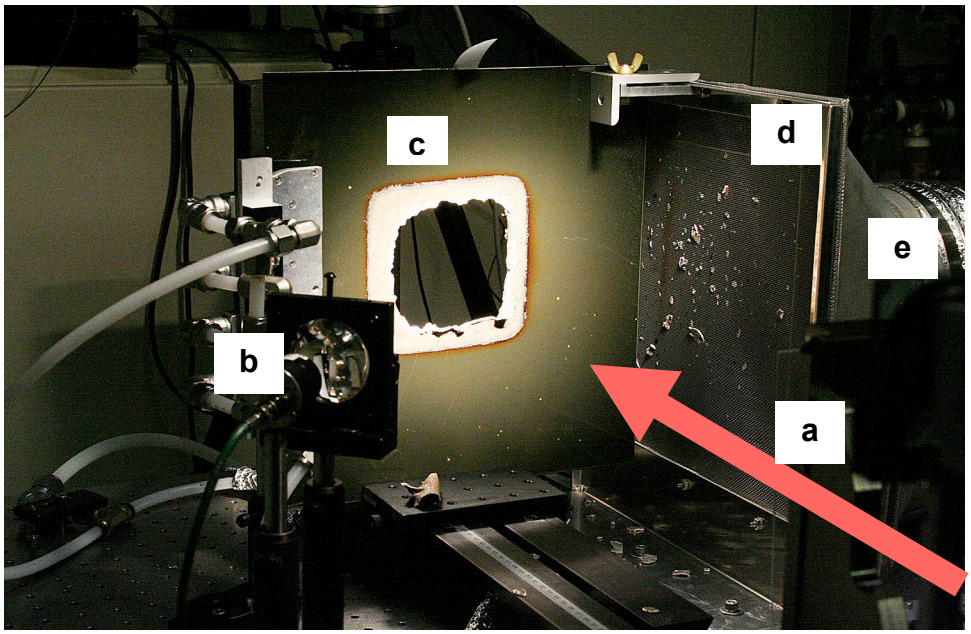

Fig. 1. Experimental setup, immediately after irradiation of a target. In this case, the spot size is 13x13 cm^2. The laser is out of view, to the lower right. The designated elements are:

(a) Beam path;

(b) Blower assembly;

(c) Target (in this case, an aluminum alloy assembly with a 13x13 cm^2 spot size);

(d) Coupon pieces on a screen;

(e) Suction assembly.

addition of a paint layer, which serves to increase the absorption. We show that THALES simulations are consistent with these observations.

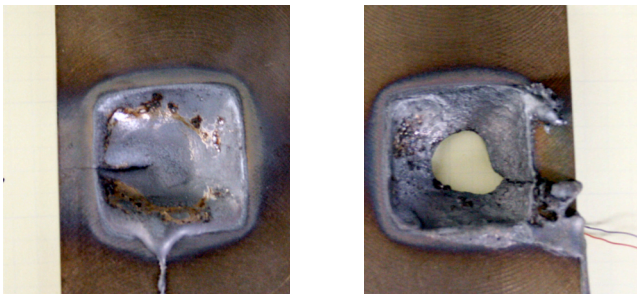

Fig. 2. Iron coupons after irradiation experiments. Left: no flow; right: airflow. The beam spot size is 3x3 cm^2.

2. Interactions with Iron Coupons

We begin by describing the irradiation of iron coupons by a beam of time-average power 25 kW, for 5 seconds. The coupon thickness was 1 cm. The spot size was a square of dimensions 3x3 cm^2, corresponding to an average intensity of about 2.8 kW/cm^2. This intensity was chosen in order to avoid significant energy losses to vaporization. The temperature history at the rear center of a coupon was recorded with a thermocouple. Experiments were conducted for three cases: (1) no flow past the surface; (2) air flow at about 100 m/s; and (3) nitrogen flow at this speed. Melt-through was observed with airflow but not with nitrogen flow or in the absence of flow. The difference between no flow and airflow is evident in the coupon photographs of Fig. 2. Note the viscous dripping under gravity in the former case.

More detailed information is revealed in the thermocouple readings shown in Figure 3. This shows that there is a striking difference between airflow and nitrogen flow. While each involves melt removal by the wind, the temperature is visibly enhanced by airflow. We attribute this to combustion. The case of no flow gives thermocouple readings similar to that of nitrogen flow. It is not considered further in this paper. Here we wish to explain the difference between

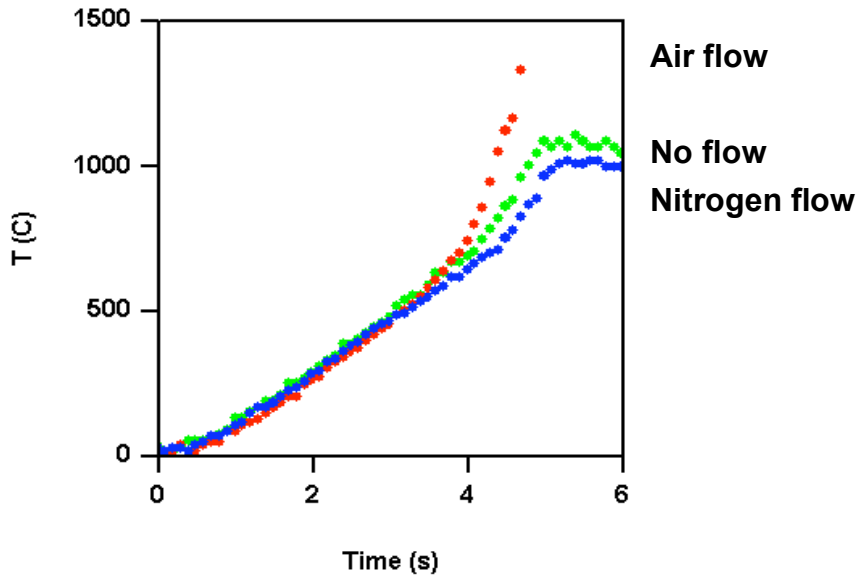

Fig. 3. Thermocouple readings for the iron coupons. The beam was turned off at 5 s.

airflow and nitrogen flow. To do so, we turn to our interaction model and add combustion effects.

Our model, THALES[5], describes physical processes within an irradiated target[3-6]. After absorption of the incident laser energy, heat is conducted through the target via the heat conduction equation,

$$\rho C \partial T / \partial t = \nabla \cdot \kappa \nabla T + S \,, \qquad (1)$$

where S is a source term particular to the problem. The wind removes melt and cools the surface. Calculations are performed in two-dimensional (r,z) symmetry, relative to the beam centerline. The model accesses a database of temperature-dependent material properties, including the heat capacity C, the thermal conductivity κ, and the absorptivity at the laser wavelength.

We have added combustion effects to this model by considering a thin oxide layer of thickness x_o, situated on a melt layer. This enters into the boundary condition for the heat conduction equation via

$$\kappa \frac{\partial T}{\partial z} = \alpha I + W_c \dot{x}_o , \tag{2}$$

where α is the surface absorptivity and W_c is the latent heat of the combustion reaction, per volume (the *z*-axis is oriented such that the temperature gradient is ordinarily positive). On a short time scale, of order ms, the oxide thickness satisfies[8]

$$\partial x_o / \partial t = (D / x_o) \exp(-T_c / T) , \tag{3}$$

where T_c is the initiation temperature and D is an empirical parameter. The solution of this equation is $x_o(t) = (2D\,t)^{1/2} \exp(-T_c / 2T)$. This is to be evaluated at the time required for melt removal, which is of order a/u, where *a* is the spot size and *u* is the melt speed at the melt surface. The latter, in turn, is of order $\sigma h / \eta$, where *h* is the melt depth, η is the shear viscosity of the melt, and σ is the shear stress at the surface. We assume a turbulent boundary layer in which the shear stress is given by the Karman expression[7], $\sigma = c \rho_0 U_0^2$, where ρ_0 and U_0 are the density and speed, respectively, of the wind. The overall factor *c* is insensitive to details of the flow. Finally, then, the boundary condition (2) takes the form

$$\kappa \frac{\partial T}{\partial z} = \alpha I + Q_c U_0 \exp(-T_c / 2T) . \tag{4}$$

Thus the heating flux due to combustion, as summarized in the last term, is proportional to the wind speed and increases exponentially with the surface temperature. Unfortunately, the parameters Q_c and T_c are not available in the literature.

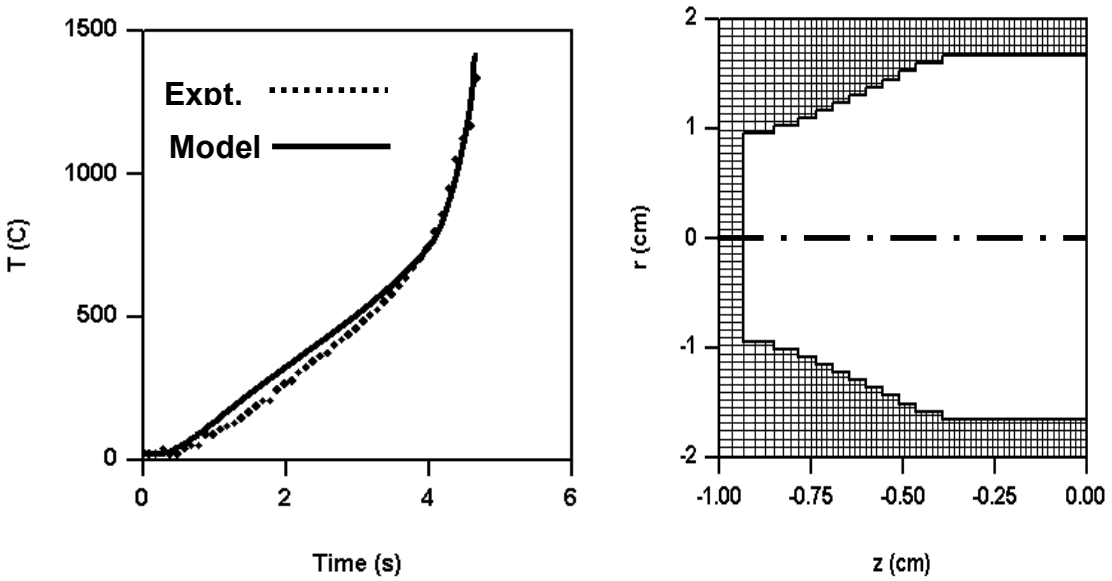

Fig. 4. Left: Comparison of experimental and calculated temperatures on rear center of iron coupon, with airflow. Right: Calculated hole profile immediately before breakthrough. A circularly symmetric geometry is used.

Figure 4 shows the thermocouple temperature as calculated by this model, with Q_c = (0.8 kW/cm^2)/(10^4 cm/s) and T_c = 4000 K. It agrees well with experiment. Overall, combustion adds approximately 35% to the deposited energy.

In Fig. 5 we show the result of a calculation with wind but without combustion. Consistently with our picture, this agrees with the laboratory result for nitrogen flow.

3. Interactions with Aluminum Coupons

Next we turn to the irradiation of aluminum coupons. Again the beam has a time-average power of 25 kW and is on for 5 s. As in the previous section, the coupon thickness was 1 cm. The temperature history at the rear center of a coupon was recorded with a thermocouple.

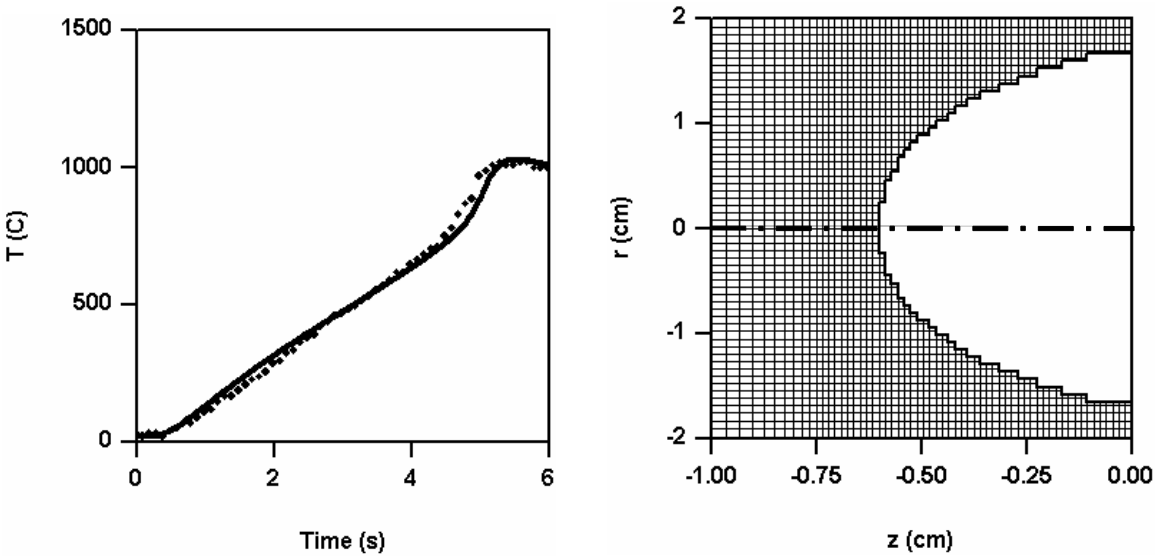

Fig. 5. Left: Comparison of experimental and calculated temperatures on rear center of iron coupon, with nitrogen flow. Right: Calculated hole profile at 5 s.

Figure 6 shows the experimental temperature trace for a spot size of 2.8x2.8 cm^2 (intensity about 3.2 kW/cm^2). During the irradiation time, the temperature grew to a maximum of about 400 C, with no melting. Also shown is the model calculation, which agrees well with the data throughout the experiment. The right-hand plot shows the temperature distribution at maximum. This clearly exhibits two-dimensional effects, owing to the large thermal conductivity. We used a mildly temperature-dependent absorptivity which increased from 0.13 at room temperature value to 0.24 at the melting point. The former value exceeds the normally quoted value of a few percent for pure aluminum, owing to surface roughness.

In the next experiment, the spot size on the coupon was decreased to 2x2 cm^2. As shown in Fig. 7, both experiment and model now give material melt-through at about 3 s.

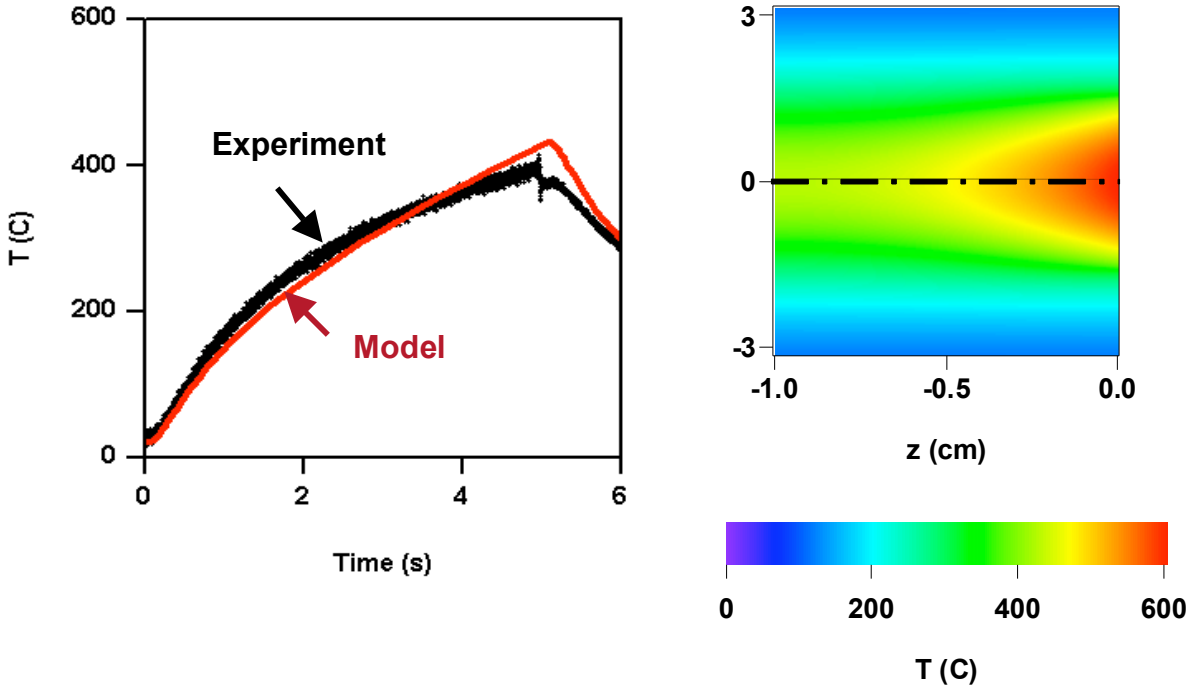

Fig. 6. Irradiation of a 1-cm aluminum coupon by 25 kW for 5 s, with a spot size of 2.8x2.8 cm^2. Left: Temperature trace of a thermocouple on rear center, along with model calculation. Right: Calculated temperature distribution immediately before the beam is turned off (beam from right).

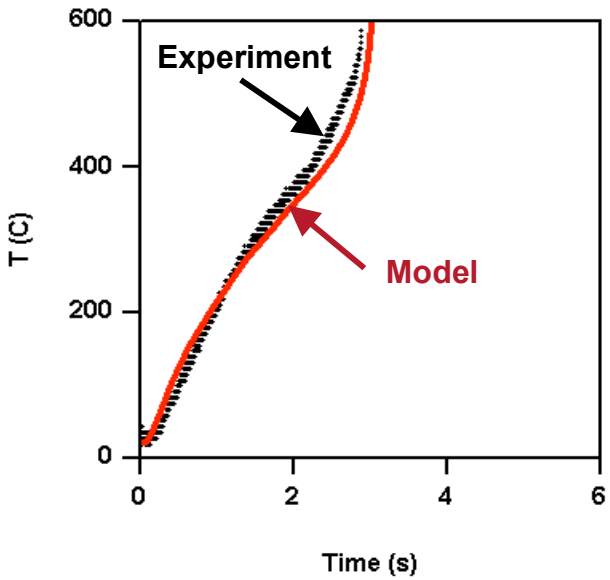

Fig. 7. Temperature trace at the rear center of an aluminum coupon, during irradiation with a spot size of 2x2 cm^2.

These experiments show that the effect of irradiating an aluminum coupon depends sensitively on the incident intensity. The reason is that the temperature profile across the target (in the beam direction) is nearly flat, owing to the large thermal conductivity. For a given irradiation time, therefore, the maximum value of this temperature is approximately proportional to the intensity. Below the melting point, there is no removal. When the intensity is high enough for the melting point to be reached, however, the entire melted volume is removed by the wind. For aluminum, incidentally, the oxide layer is sufficiently dense to block oxygen access to the surface, so combustion is not important.

In practice, the sensitivity to intensity is smoothed by the fact that targets are usually painted. From an elementary point of view, paint acts as a thin layer with a high absorptivity and a low thermal conductivity. To see the effect, we irradiated a painted coupon, with a spot size of 3x3 cm^2, for 5 s. The paint was a dull grey. Recall that a slightly smaller spot size, 2.8x2.8 cm^2, failed to produce melting. The painted coupon, however, absorbed appreciably more energy and melted through somewhat after 2 s, as shown in Fig. 8. (The thermocouple failed at 2 s, because of the loss of material strength below melting temperature.) This experiment suggests that the paint survived up to the point at which the aluminum began to melt. As a result, a painted layer greatly decreases the power required to drill through an aluminum target.

Also shown in Fig. 8 is the result of a THALES calculation, in which the paint was treated as a 200-μm layer with an absorptivity of 0.8 and a thermal conductivity of 0.08 W/cm K. The paint mostly survived until the aluminum melting point was reached, and the temperature trace is reasonably close to experiment. These confirm that our simple model of this paint may be adequate.

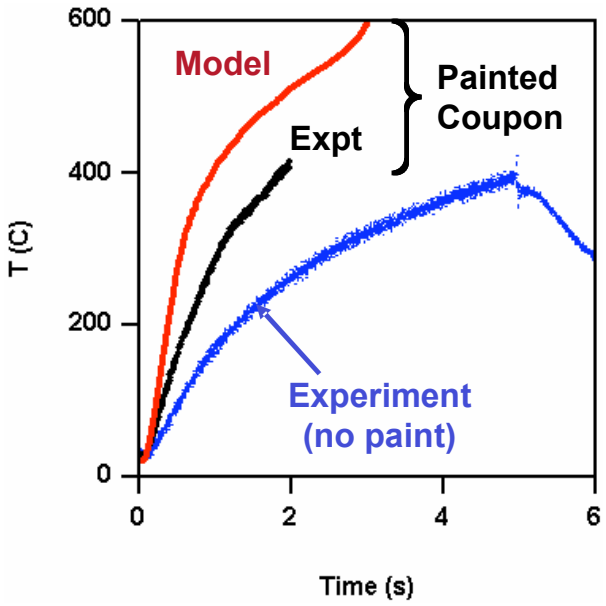

Figure 8. Black line: Thermocouple trace for the irradiation of a 1-cm painted aluminum coupon by 25 kW for 5 s, with a spot size of 3x3 cm^2. The thermocouple failed at 2 s. The red line gives the model prediction. The blue line gives the temperature trace for a 2.8x2.8 cm^2 spot with no paint, from Fig. 6.

4. Conclusions

We have described experiments and modeling concerning the interactions of a high-power solid-state laser with target materials. The laser delivered 25 kW for 5 s, on coupons of iron and aluminum having a thickness of 1 cm. The spot sizes were relatively large, about 3x3 cm^2, and airflow at about 100 m/s was present. For an iron coupon, we showed that combustion plays an important role in adding to the material heating. This effect was absent in nitrogen flow.

For aluminum, we found a strong dependence on the incident laser intensity. At approximately 3.2 kW/cm^2, no melting was observed, because of efficient lateral heat conduction. At about 6.2 kW/cm^2, however, the coupon rapidly melted through. This behavior was explained in terms of rapid heat conduction along the axial direction. Paint was observed to increase appreciably the absorption and thus to decrease the power needed for melt-through. We showed that all these results are reproduced by a comprehensive computational model.

Finally, it should be noted that this phenomenology does not apply to iron, for which the thermal diffusivity is about an order of magnitude lower than aluminum, depending on the temperature. In iron, the temperature typically has a strong gradient near the edge. Consequently, a thin melted layer is continuously removed by the wind. A painted layer would not be expected to have a strong effect on laser penetration.

Acknowledgments

We are pleased to acknowledge our indebtedness to the project manager of the LLNL high average power laser program, R. M. Yamamoto.

References

[1]Boley, C. D., and A. M. Rubenchik, "Modeling of Material Removal by Solid State Heat Capacity Lasers," Proc. 15th Annual Solid State and Diode Laser Technology Review, Albuquerque, NM, June 3-6, 2002.

[2]Boley, C. D., and A. M. Rubenchik, "Modeling of High-Energy Pulsed Laser Interactions with Coupons," University of California, UCRL-ID-151857, Feb. 6, 2003.

[3]Boley, C. D., and A. M. Rubenchik, "Simulations of Target Interactions with Pulsed, High-Energy Laser," Proc. 17th Annual Solid State and Diode Laser Technology Review, Albuquerque, NM, June 8-10, 2004.

[4]Boley, C. D., and A. M. Rubenchik, "Lethality of High-Power Solid-State Lasers on High-Explosive Targets," Eighth Annual Directed Energy Symposium, Lihue, HI, Nov. 14-18, 2005.

[5]Boley, C. D., and A. M. Rubenchik, "Modeling of Antimortar Lethality by a Solid-State Heat-Capacity Laser," J. Directed Energy **2**, 97-106 (2006).

[6]Boley, C. D., S. N. Fochs, and A. M. Rubenchik, "Lethality of a High-Power Solid-State Laser," Ninth Annual Directed Energy Symposium, Albuquerque, NM, Oct. 30 – Nov. 3, 2006.

[7]Landau, L. D., and E. M. Lifshitz, "Fluid Mechanics," Pergamon Press, 1978.

[8]Prokhorov, A. M., V. I. Konov, I. Ursu, and I. N. Mihailescu, "Laser Heating of Metals," Adam Hilger, 1990.

[9]Soules, T. F., et al., "Ceramic Nd:YAG – Current Material of Choice for SSHCL," Eighth Annual Directed Energy Symposium, Lihue, HI, Nov. 14-18, 2005.

[10]Yamamoto, R. M., *et al.*, "Laser Performance of the Solid-State Heat-Capacity Laser (SSHCL)," Ninth Annual Directed Energy Symposium, Albuquerque, NM, Oct. 30 – Nov. 3, 2006.